Experimental optical retrieval of the Thermal Boundary Resistance of carbon nanotubes in water

Carbon 229 (2024) 119445

Contents lists available at ScienceDirect

Carbon

journal homepage: www.elsevier.com/locate/carbon

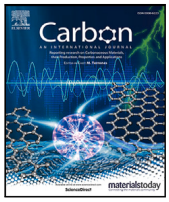

Research paper

Experimental optical retrieval of the Thermal Boundary Resistance of carbon nanotubes in water

Alessandro Casto [a], Margherita Vittucci [a], Fabien Vialla [a], Aurélien Crut [a], Francesco Maria Bellussi [b], Matteo Fasano [b], Fabrice Vallée [a], Natalia Del Fatti [a,c], Francesco Banfi [a], Paolo Maioli [a,*]

[a] Université Claude Bernard Lyon 1, CNRS, Institut Lumière Matière, UMR5306, F-69622, Villeurbanne, France
[b] Politecnico di Torino, Department of Energy, Corso Duca degli Abruzzi 24, 10129, Torino, Italy
[c] Institut Universitaire de France (IUF), France

ARTICLE INFO

Keywords:
Carbon nanotubes
Water
Thermal Boundary Resistance
Nanofluids
Heat transfer
Time-resolved spectroscopy

ABSTRACT

Carbon-based nanostructures are extensively employed as solid additives in nanofluids or polymer matrices for applications in light harvesting, energy conversion and storage. To predict heat transfer in carbon-based nanostructures, a quantitative comprehension of thermal energy exchanges at the interface with their external environment is crucial. The Thermal Boundary Resistance (TBR) stands out as a key parameter hindering efficient thermal energy exchanges between nano-objects and their surroundings. In this work we experimentally determine the TBR for the archetypal case of an interface between multi-wall carbon nanotubes (CNTs) and water. Ultrafast energy exchanges are investigated using femtosecond time-resolved optical spectroscopy. Data rationalization via a thermo-optical model allows retrieval of a CNT/water interface TBR of $(4.6 \pm 2.2)\times10^{-8}$ m^2K/W. This value constitutes a benchmark for theories aimed at understanding energy transfer between a CNT and water. Notably, the functionalization of the surface of CNTs with covalent groups has been demonstrated to reduce the TBR and facilitate solid–liquid heat exchanges. The measurement and analysis protocol developed in this study is versatile and can be applied to any nanofluid and nanocomposite material.

1. Introduction

Carbon nanotubes (CNTs) are extensively employed for mechanical and thermal optimization of composite materials [1–5]. Dispersed in water they can give rise to improved coolant fluids for heat exchangers [6]. Superfast water flow inside CNTs [7] makes them apt for wastewater disinfection treatment [8], desalination membranes [9] and water transport control [10,11], while their large surface over volume ratio opens the way to their use as nanosized heat sinks [12,13]. Due to their broad optical absorption spectrum, CNTs in water are also preferred to metal nanoparticles as photothermal agents in applications requiring large energy absorption in nanoscale volumes [14] and are potential candidates for photoacoustic applications [15]. In all these scenarios, it is crucial to regulate the rate of heat transfer at the CNT/water interface. This rate is governed by the Thermal Boundary Resistance (TBR), also referred to as Kapitza resistance [16]. This resistance arises from the mismatch in atomic positions on both sides of the interface, combined with variations in the elastic properties of the two materials. The TBR stands out among the limiting factors in nanofluids heat transfer, the issue being particularly critical for nanofluids with high density of nanoparticles.

However, retrieval of the TBR from static measurements is challenging, since they introduce spurious contact resistances that add in series to the TBR and are of the same order of magnitude [17]. Ultrafast time-resolved optical spectroscopy – a far-field, low perturbation, non contact technique – emerges as a viable alternative to access nanoscale heat transfer [18–28]. A key issue though stands in the interpretation of the transient optical signals, which are not necessarily proportional to the temperature of the excited nano-objects and may be strongly influenced by the temperature dynamics of the environment [25–28]. On the chemistry side, hydrophobicity of bare CNTs makes them unstable in water, with a tendency to agglomerate into bundles which precipitate [29,30]. To overcome this issue, surfactants are frequently used for CNT stabilization in water. However, they modify the interface, hence the energy flux across it, ultimately affecting the TBR [31]. Due to the above-mentioned difficulties, heat transfer between bare CNTs

* Corresponding author.
E-mail address: paolo.maioli@univ-lyon1.fr (P. Maioli).

https://doi.org/10.1016/j.carbon.2024.119445
Received 12 April 2024; Received in revised form 24 June 2024; Accepted 12 July 2024
Available online 18 July 2024

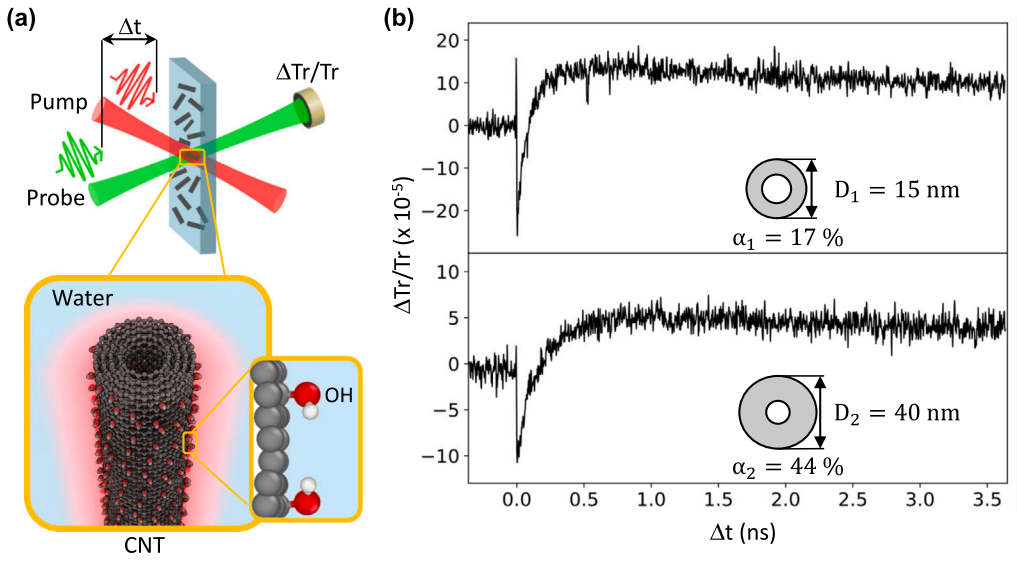

Fig. 1. (a) Top: outline of the setup for ultrafast spectroscopy, with red pump pulses, which photoexcite a solution containing CNTs dispersed in water, and green probe pulses with a controlled time delay (Δt), detected with a photodiode and a lock-in amplifier. Bottom: representation of a multi-wall CNT in water and zoom on its surface partially covered by -OH groups covalently bound to C atoms. (b) Relative differential transmission variation ΔTr/Tr of the two samples in solution as a function of pump–probe delay Δt, with pump and probe wavelength $\lambda_{pp} = 800$ nm and $\lambda_{pr} = 530$ nm respectively. Insets: samples dimensions and -OH coverage fraction α.

(or graphene) and water have mostly been investigated theoretically via molecular dynamics simulations (MD) [32–38].

We here report on the first experimental determination of the TBR at the interface between bare CNTs and water using optical ultrafast spectroscopy. The strategy employed for retrieving the TBR at the bare carbon/water interface consists in investigating two different samples of water-dispersed multi-wall CNTs, both partially covered by covalently bound -OH functional groups so as to avoid CNTs aggregation. Two different surface coverage fractions α are used, with α defined as the ratio between the number of carbon atoms bonded to -OH groups over the total number of carbon atoms composing the external CNT surface. CNT surface modification by functional groups is indeed expected to have a significant impact on the heat transfer at the interface [39–42]. For each of the two coverage fractions, we experimentally retrieve an *effective* TBR. This is extracted by fitting the time-resolved optical traces with a full thermo-optical model which accounts for thermal and optical dynamics of both the CNTs and the environment. The effective TBR is the parallel resistance between the TBR at the surface portion covered by -OH groups (CNT-OH/water interface, surface coverage fraction α), noted $R_{CNT\text{-}OH/H_2O}$, and the TBR at the surface portion where C atoms are in direct contact with water molecules (CNT/water interface, surface coverage fraction $1-\alpha$), noted R_{CNT/H_2O}. By measuring the effective TBR in the two samples with different surface coverage fraction we extract the TBR at both bare CNT/water and CNT-OH/water interfaces.

2. Experimental methods

The two investigated multi-wall CNTs samples are sample 1, with outer diameter $D_1 = (15 \pm 5)$ nm, inner diameter (7.5 ± 2.5) nm, and $\alpha_1 = 17 \pm 1\%$ and sample 2, with outer diameter $D_2 = (40 \pm 10)$ nm, inner diameter (8.5 ± 2.5) nm and $\alpha_2 = 44 \pm 2\%$. All CNTs have ~1-μm length and are supplied as powders, which are dispersed in ultrapure water until optimal concentration for optical investigations is reached (optical density from 0.5 to 1 in a 1-mm optical path cuvette, which corresponds to a CNT concentration $n_{CNT} \sim 10^8$ mm^{-3}).

Fig. 1a schematizes the ultrafast time-resolved technique and the layout of the investigated samples. A first laser pulse (pump) is used to impulsively excite the solution containing CNTs. A second time-delayed laser pulse (probe) allows to measure the transient variations of the sample optical absorption. We used an amplified Ti:Sa femtosecond laser, with 250 kHz repetition rate, and 400–850 nm wavelength tunability by combination with an optical parameter amplifier. At the sample, pump pulses have a fluence around ~5 mJ/cm^2 and a diameter ~30 μm. We experimentally access the variation of the relative optical transmission ΔTr/Tr of the solutions containing the CNTs as a function of the pump–probe delay Δt, as shown in Fig. 1b. Transient optical signals are the result of a sudden electron out-of-equilibrium excitation triggered by the pump pulse, which is followed by charge carrier relaxation by internal thermalization and electron energy loss to the lattice. These processes occur in the first few picoseconds and have been extensively investigated both in bulk [43,44] and nanoscale systems [18,45–48]. Also in the present case, these ultrashort dynamics occur within the first few picoseconds (Fig. 1b) and will not be further addressed. We pinpoint that water is transparent at the pump and probe laser wavelengths.

3. Results and discussion

For our purposes, we will focus beyond the few picosecond timescale. After a few picoseconds a thermodynamic temperature is indeed defined for the CNT as a whole [19–22,24–28,49]. Subsequently, the CNT temperature decreases, heat being transferred to water. On both samples the signals show two relaxation dynamics. A first decay, from negative to positive ΔTr/Tr values, occurs in the first hundreds of picoseconds; a second decay brings the signal back to equilibrium on the few nanoseconds timescale. Interestingly, the ΔTr/Tr signal contributions from the two relaxation dynamics have opposite signs, mostly negative for the first decay and positive for the second one. A biexponential fit yields two different relaxation time-constants for the first decay : $\tau_{s1} \approx 100$ ps and $\tau_{s2} \approx 200$ ps for samples 1 and 2, respectively.

Often the decay time in the time-resolved signals is qualitatively related to the thermal problem adopting a lumped thermal model [50,51], which assumes that the environment, *i.e.* water, remains isothermal during the CNT cooling process, and ΔTr/Tr is proportional to the nano-object, *i.e.* the CNT, temperature only. For the case of a carbon-filled CNT, this line of thought leads to a single decay time $\tau = R \cdot c \cdot V/S$ [19], where R is the value of the TBR, c the CNT specific heat, V the volume and S the external surface of the CNT. Although appealing for the vivid physical picture it yields, the above mentioned expression is not applicable in the present setting. Regarding the thermics, water

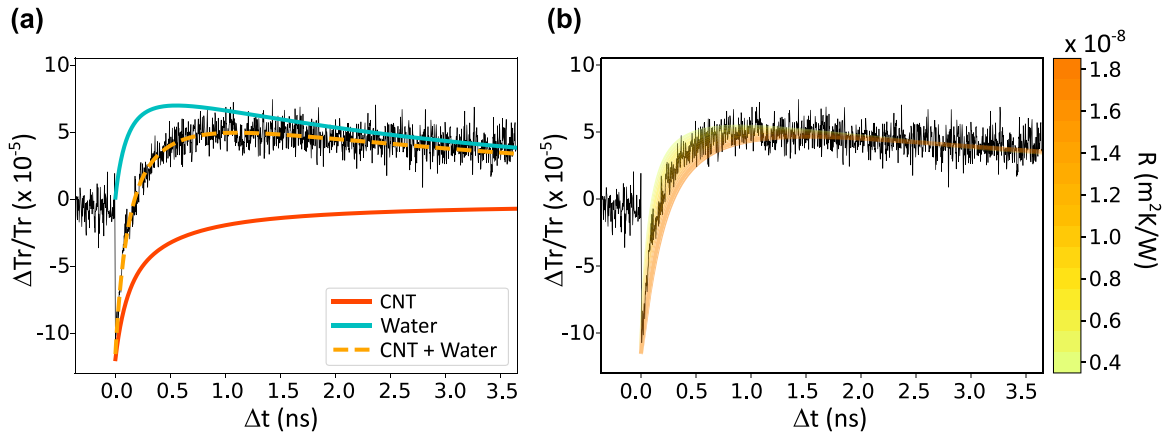

Fig. 2. (a) Time-resolved relative transmission change (black line) from sample 2 with 800 nm pump and 530 nm probe pulses (same as in Fig. 1b), and signal computed using the thermo-optical model (dashed orange line) with a TBR value $R_2 = 1.3 \times 10^{-8}$ m^2 K/W. Red and blue lines: contributions of CNT and water temperature dynamics respectively to the modeled optical signal. (b) Simulated signals with different values of TBR (lines from yellow to orange) superposed to the experimental trace.

does not maintain a uniform temperature throughout the CNT cooling process. On the optical side, ΔTr/Tr is not ruled by the CNT temperature dynamics only, as clearly indicated by the two exponential dynamics. Hence, in order to precisely extract the TBR, a complete thermo-optical model is here developed.

The model reproduces both (1) the temperature dynamics of the CNT and its surroundings and (2) the induced transient variations of the optical signals, to be compared against experiments [25,26]. The model, solved numerically by Finite Element Method (FEM) [27,28], is as follows. In the case of identical and equally-oriented CNTs, the optical time-resolved signal reads $\Delta\mathrm{Tr/Tr}(\lambda_{pr}, \Delta t) = -n_{CNT} L \Delta\sigma_{ext}(\lambda_{pr}, \Delta t)$, with λ_{pr} the wavelength of the probe pulse, L the optical path within the cuvette where the pump and probe beams intersect, n_{CNT} the number density of CNTs in the sample and $\Delta\sigma_{ext}$ the photo-induced variation of the optical extinction (accounting for both absorption and scattering) cross-section of a single CNT [18]. $\Delta\sigma_{ext}$ depends on the properties of both the nano-object and its local environment, namely: (1) temperature variation of CNTs, which modifies the real and imaginary dielectric permittivities, $\Delta\epsilon_1$ and $\Delta\epsilon_2$, respectively, [25] and (2) temperature dynamics of water refractive index, through the real water permittivity $\Delta\epsilon_w$, its imaginary part being negligible within our wavelengths range. $\Delta\sigma_{ext}(\lambda_{pr}, \Delta t)$ is thus a function of $\Delta\epsilon_1(\lambda_{pr}, \Delta t)$, $\Delta\epsilon_2(\lambda_{pr}, \Delta t)$ and $\Delta\epsilon_w(\lambda_{pr}, \Delta t)$, their contributions depending on the particle composition, morphology and orientation with respect to light polarization [18,26,52].

Throughout the modeling, uniform excitation and probing of all CNTs are assumed, as the laser spot size is around 30 μm, *i.e.* well in excess of the CNT length ~1 μm. Only thermal transfer in the radial direction is considered, as the CNTs length is much higher than their diameter. Thermal cross-talk among different CNTs is neglected. In fact, the thermal diffusion length out of the CNTs, within the maximum measurement time delay $t_{max} = 4$ ns, is $\sqrt{D t_{max}} \sim 20$ nm (with D water thermal diffusivity), much shorter than CNTs interdistance ~2 μm. Cumulative excitation effects are ignored as the delay (4 μs) between subsequent pulses is much longer than CNT cooling dynamics. Solution of the thermo-optical model is based on three successive steps. (1) FEM computations of the diameter-dependent optical absorption cross section $\sigma_{abs}(\lambda_{pp})$ per unit length of a CNT, with λ_{pp} the pump-beam wavelength. Note that the model accounts for the random CNT orientation with respect to the pump light polarization [52]. Computation of $\sigma_{abs}(\lambda_{pp})$ requires input of the wavelength-dependent dielectric permittivities $\epsilon_{1,2,w}(\lambda_{pp})$ [53] at room temperature, and leads to the estimation of the orientation-dependent pump-induced initial temperature increase of the CNT [18], here up to a few hundred Kelvin [15]. (2) Computation of the full temperature dynamics of both CNT and surrounding water, $\Delta T_{CNT}(\Delta t)$ and $\Delta T_w(\Delta t, r)$ respectively [25,26,54], where r is the distance from the nanotube axis. This entails two factors: Fourier heat diffusion within CNTs and within water, as well as the TBR at the interface between CNTs and water. The temperature inside the CNT is almost uniform, due to its high thermal conductivity, and it monotonically decreases while transferring heat to water. The temperature of the water outside CNTs increases accordingly and subsequently returns to equilibrium [25,26]. The water contained inside the CNT reaches the temperature of the CNTs within a few tens of picoseconds and remains thermally linked to the CNTs thereafter [15]. Note that TBR value at the internal interface has negligible influence on the thermal dynamics of the CNTs. The value of the TBR at the external interface, which is the free parameter to be determined by fitting the experimental signals, as well as the specific heats and thermal conductivities of CNT (considered equivalent to that of bulk graphite) and water, which are known, completely fix these thermal dynamics. (3) By introducing the thermal dependence of carbon and water dielectric permittivities $\epsilon_{1,2,w}$ [53,55–57], we can estimate their time and spatial dependence. This leads to the complete determination of $\Delta\sigma_{ext}(\lambda_{pr}, \Delta t)$, after averaging the optical signals over all the CNT orientations. Comparing $\Delta\sigma_{ext}(\lambda_{pr}, \Delta t)$ to the experimental $\Delta\mathrm{Tr/Tr}(\lambda_{pr}, \Delta t)$ enables the extraction of the TBR, which, aside from an amplitude factor, represents the sole free parameter within the model.

Superposition of the experimental signal from sample 2 and the modeled one (upon insertion of the optimal TBR fitting value), is shown in Fig. 2a (dashed line), after multiplication of the simulated $\Delta\sigma_{ext}(\Delta t)$ trace by a negative amplitude factor (corresponding to $-n_{CNT}L$) for comparison with the experimental ΔTr/Tr. The two contributions of CNT and water temperature dynamics to the optical signal, $\Delta\sigma_{ext,CNT}$ and $\Delta\sigma_{ext,w}$, respectively, are also shown individually (red and blue lines respectively).[1] $\Delta\sigma_{ext,CNT}(\Delta t)$ is proportional to $\Delta T_{CNT}(\Delta t)$ and decays monotonically, reflecting CNT cooling to equilibrium after the initial photoinduced heating. The dependence of $\Delta\sigma_{ext,w}(\Delta t)$ on $\Delta T_w(\Delta t, r)$ is intricate, given that water temperature varies not only with time but also spatially. $\Delta\sigma_{ext,w}(\Delta t)$ shows indeed a more complex profile, with an initial increase, which is due to proximal water heating by the heat transferred from the CNT, and subsequent cooling to equilibrium, by heat diffusion to the water volume far from the CNT. This analysis demonstrates the necessity of considering water temperature dynamics to accurately replicate the transient optical response of the system, despite water being non-absorbing in the visible spectrum. Heating of

[1] The individual contribution of the CNT (water) temperature dynamics to the optical signal, $\Delta\sigma_{ext,CNT}$ ($\Delta\sigma_{ext,w}$), is calculated imposing a temperature-independent water dielectric function ϵ_w (temperature-independent CNT dielectric function ϵ_1 and ϵ_2).

water induces a modification of $\Delta\epsilon_w(\Delta t, r)$ and modifies, by a local environment refractive index effect, the optical extinction of the absorbing CNT [25,26]. Incorporating water dynamics is crucial for achieving an accurate fit of the CNT cooling dynamics and obtaining a quantitative estimation of the CNT/water TBR.

Initially, at $\Delta t = 0$, the contribution from water is negligible since only the temperature of the CNT is directly influenced by the excitation. The optical response is impacted by the CNT contribution (red line) for short delays, while the latter becomes negligible for longer delays. Variations in the TBR are thus expected to primarily affect the signal on the short timescale. We systematically simulated time-resolved signals spanning over several values of TBR (Fig. 2b). The best fitted TBR values are $R_1 = (2.3 \pm 0.2) \times 10^{-8}$ m^2 K/W and $R_2 = (1.3 \pm 0.2) \times 10^{-8}$ m^2 K/W for sample 1 and 2, respectively.

For the relatively large CNT sizes considered here, the nano-object curvature is not supposed to affect the TBR, as supported by predictions from MD simulations [34,58,59]. The difference in the TBR between the two samples cannot thus be explained by their different diameters and is attributed to the different -OH coverage of the two samples. For a fixed value of α, the total heat flux from the CNT to water is given by the weighted sum of the heat flux across the CNT-OH/water (surface coverage α) and that across the CNT/water (surface coverage $1-\alpha$) interface. The effective TBR is hence the equivalent thermal resistance of $R_{CNT\text{-}OH/H_2O}$ (with weight α) in parallel with R_{CNT/H_2O} (with weight $1-\alpha$), refer to inset of Fig. 3. The effective TBRs in the two measured samples thus read:

$$\frac{1}{R_1} = \frac{1-\alpha_1}{R_{CNT/H_2O}} + \frac{\alpha_1}{R_{CNT\text{-}OH/H_2O}}$$
$$\frac{1}{R_2} = \frac{1-\alpha_2}{R_{CNT/H_2O}} + \frac{\alpha_2}{R_{CNT\text{-}OH/H_2O}}. \quad (1)$$

Solving the system of two equations for the two unknowns we obtain $R_{CNT/H_2O} = (4.6 \pm 2.2) \times 10^{-8}$ m^2 K/W and $R_{CNT\text{-}OH/H_2O} = (0.7 \pm 0.2) \times 10^{-8}$ m^2 K/W. Representation of the two experimental values of thermal conductance as a function of the -OH functionalization fraction α (Fig. 3) allows to directly visualize the two asymptotic values and their error bars.

TBR values, numerically computed by Molecular Dynamics on carbon-based materials in water, span from 1.2 to 35 $\times 10^{-8}$ m^2 K/W [15,33,34,38,60,61]. The wide range observed is attributed to the inherent variability in molecular dynamics (MD) computations, including the selection of specific force-field potentials and the methodology used to extract the Thermal Boundary Resistance (TBR) from a set of equilibrium or out-of-equilibrium MD simulations [38]. This further calls for an experimental value of the TBR against which any theoretical value could be benchmarked. The value $R_{CNT/H_2O} = (4.6 \pm 2.2) \times 10^{-8}$ m^2 K/W we report here serves the scope.

As evidenced in Fig. 3, CNT functionalization with -OH reduces the value of the TBR, *i.e.* it accelerates interfacial thermal transport due to a *graded* acoustic impedance mismatch across the interface. Elastic properties of the -OH interfacial layer are indeed intermediate between the ones of CNTs and of water [40]. Similar trends have been theoretically predicted by MD for functionalized graphene sheets immersed in water [40], paraffin [39], and oil [62].

4. Conclusions

To summarize, we established the experimental value of the TBR at the bare CNT/water interface merging ultrafast time-resolved spectroscopy, a full thermo-optical FEM model and performing measurements on two samples of multi-wall CNTs with different surface coverage fractions by -OH groups. The TBR value bears great relevance as it will allow to make predictions on the effective thermal resistivity of nanofluids based on water and with carbon-based nanofillers. This holds crucial importance across a spectrum of energy-related applications, spanning from solar energy harvesting and energy conversion to storage and desalination. From a fundamental scientific perspective, the value reported here serves as a benchmark for theories aiming to rationalize heat transfer at the interface between carbon nanotubes and water. Furthermore, our findings demonstrate that the effective TBR can be adjusted by varying the concentration of -OH groups. The protocol outlined in this study is highly versatile and can be readily applied to any nanofluid and solid nanocomposite beyond those composed of water and/or CNTs, thereby extending the impact of these findings to energy transfer in nanofluids and nanocomposite materials on a wide scale. Specifically, the investigations detailed here are being expanded to include MWCNTs in different environments, such as ethanol, aqueous solutions with varying pOH levels, and polymeric matrices.

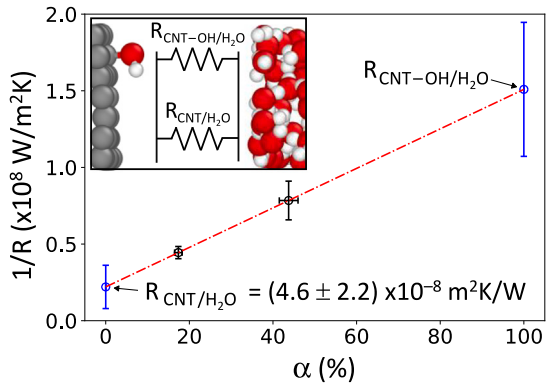

Fig. 3. Experimental values of Thermal Boundary Conductance (black dots) in samples 1 and 2 are used to retrieve the values of R_{CNT/H_2O} and $R_{CNT\text{-}OH/H_2O}$ (blue dots) which correspond to an interface entirely free ($\alpha = 0\%$) or fully covered by -OH groups ($\alpha = 100\%$) respectively. Red line is a linear fit to experimental data (see main text for the procedure for R_{CNT/H_2O} and $R_{CNT\text{-}OH/H_2O}$ extraction). In the inset, representation as a function of two thermal resistances in parallel between CNT surface (left) and water (right).

CRediT authorship contribution statement

Alessandro Casto: Writing – review & editing, Writing – original draft, Visualization, Validation, Software, Investigation, Formal analysis, Data curation, Conceptualization. **Margherita Vittucci:** Writing – review & editing, Visualization, Investigation, Formal analysis, Data curation. **Fabien Vialla:** Writing – review & editing, Visualization, Methodology. **Aurélien Crut:** Writing – review & editing, Methodology, Funding acquisition, Data curation. **Francesco Maria Bellussi:** Writing – review & editing, Visualization, Methodology. **Matteo Fasano:** Writing – review & editing, Visualization, Methodology, Conceptualization. **Fabrice Vallée:** Writing – review & editing, Funding acquisition. **Natalia Del Fatti:** Writing – review & editing, Visualization, Validation, Supervision, Funding acquisition, Conceptualization. **Francesco Banfi:** Writing – review & editing, Visualization, Validation, Methodology, Data curation, Conceptualization. **Paolo Maioli:** Writing – review & editing, Writing – original draft, Visualization, Validation, Supervision, Project administration, Methodology, Investigation, Funding acquisition, Formal analysis, Data curation, Conceptualization.

Declaration of competing interest

The authors declare that they have no known competing financial interests or personal relationships that could have appeared to influence the work reported in this paper.

Acknowledgments

This work was supported by the French National Research Agency (ANR) under the reference ANR-20-CE30-0016 (ULTRASINGLE project).

References

[1] Y. Cai, H. Yu, C. Chen, Y. Feng, M. Qin, W. Feng, Improved thermal conductivities of vertically aligned carbon nanotube arrays using three-dimensional carbon nanotube networks, Carbon 196 (2022) 902–912.

[2] S. Zhang, Y. Ma, L. Suresh, A. Hao, M. Bick, S.C. Tan, J. Chen, Carbon nanotube reinforced strong carbon matrix composites, ACS Nano 14 (8) (2020) 9282–9319.

[3] W. Yu, C. Liu, S. Fan, Advances of CNT-based Systems in thermal management, Nano Res. 14 (2021) 2471–2490.

[4] K. Chawla, J. Cai, D. Thompson, R. Thevamaran, Superior thermal transport properties of vertically aligned carbon nanotubes tailored through mesoscale architectures, Carbon 216 (2024) 118526.

[5] F. Zhang, Y. Sun, L. Guo, Y. Zhang, D. Liu, W. Feng, X. Shen, Q. Zheng, Microstructural welding engineering of carbon nanotube/polydimethylsiloxane nanocomposites with improved interfacial thermal transport, Adv. Funct. Mater. 34 (2024) 2311906.

[6] M.U. Sajid, H.M. Ali, Recent advances in application of nanofluids in heat transfer devices: a critical review, Renew. Sustain. Energy Rev. 103 (2019) 556–592.

[7] E. Secchi, S. Marbach, A. Niguès, D. Stein, A. Siria, L. Bocquet, Massive radius-dependent flow slippage in carbon nanotubes, Nature 537 (7619) (2016) 210–213.

[8] B. Arora, P. Attri, Carbon nanotubes (CNTs): a potential nanomaterial for water purification, J. Compos. Sci. 4 (3) (2020) 135.

[9] R. Wang, D. Chen, Q. Wang, Y. Ying, W. Gao, L. Xie, Recent advances in applications of carbon nanotubes for desalination: A review, Nanomaterials 10 (6) (2020) 1203.

[10] J. Leng, T. Ying, Z. Guo, Y. Zhang, T. Chang, W. Guo, H. Gao, Thermally induced continuous water flow in long nanotube channels, Carbon 191 (2022) 175–182.

[11] M. Fasano, E. Chiavazzo, P. Asinari, Water transport control in carbon nanotube arrays, Nanoscale Res. Lett. 9 (1) (2014) 559.

[12] Z. Huang, M. Gao, T. Pan, Y. Zhang, B. Zeng, W. Liang, F. Liao, Y. Lin, Microstructure dependence of heat sink constructed by carbon nanotubes for chip cooling, J. Appl. Phys. 117 (2) (2015) 024901.

[13] R. Cao, S. Chen, Y. Wang, N. Han, H. Liu, X. Zhang, Functionalized carbon nanotubes as phase change materials with enhanced thermal, electrical conductivity, light-to-thermal, and electro-to-thermal performances, Carbon 149 (2019) 263–272.

[14] G. Baffou, F. Cichos, R. Quidant, Applications and challenges of thermoplasmonics, Nature Mater. 19 (9) (2020) 946–958.

[15] M. Diego, M. Gandolfi, A. Casto, F.M. Bellussi, F. Vialla, A. Crut, S. Roddaro, M. Fasano, F. Vallée, N. Del Fatti, et al., Ultrafast nano generation of acoustic waves in water via a single carbon nanotube, Photoacoustics 28 (2022) 100407.

[16] E.T. Swartz, R.O. Pohl, Thermal boundary resistance, Rev. Modern Phys. 61 (1989) 605–668.

[17] Y. Xian, P. Zhang, S. Zhai, P. Yuan, D. Yang, Experimental characterization methods for thermal contact resistance: A review, Appl. Therm. Eng. 130 (1) (2018) 1530–1548.

[18] T. Stoll, P. Maioli, A. Crut, N. Del Fatti, F. Vallée, Advances in femto-nano-optics: ultrafast nonlinearity of metal nanoparticles, Eur. Phys. J. B 87 (11) (2014) 260.

[19] S.T. Huxtable, D.G. Cahill, S. Shenogin, L. Xue, R. Ozisik, P. Barone, M. Usrey, M.S. Strano, G. Siddons, M. Shim, et al., Interfacial heat flow in carbon nanotube suspensions, Nature Mater. 2 (11) (2003) 731–734.

[20] S.D. Kang, S.C. Lim, E.-S. Lee, Y.W. Cho, Y.-H. Kim, H.-K. Lyeo, Y.H. Lee, Interfacial thermal conductance observed to be higher in semiconducting than metallic carbon nanotubes, ACS Nano 6 (2012) 3853–3860.

[21] J. Park, D.G. Cahill, Plasmonic sensing of heat transport at solid–liquid interfaces, J. Phys. Chem. C 120 (2016) 2814–2821.

[22] A. Beardo, J.L. Knobloch, L. Sendra, J. Bafaluy, T.D. Frazer, W. Chao, J.N. Hernandez-Charpak, H.C. Kapteyn, B. Abad, M.M. Murnane, F.X. Alvarez, J. Camacho, A general and predictive understanding of thermal transport from 1D- and 2D-confined nanostructures: Theory and experiment, ACS Nano 15 (8) (2021) 13019–13030.

[23] B.T. Diroll, A. Brumberg, A.A. Leonard, S. Panuganti, N.E. Watkins, S.A. Cuthriell, S.M. Harvey, E.D. Kinigstein, J. Yu, X. Zhang, M.G. Kanatzidis, M.R. Wasielewski, L.X. Chen, R.D. Schaller, Photothermal behaviour of titanium nitride nanoparticles evaluated by transient X-ray diffraction, Nanoscale 13 (4) (2021) 2658–2664.

[24] V. Juvé, M. Scardamaglia, P. Maioli, A. Crut, S. Merabia, L. Joly, N. Del Fatti, F. Vallée, Cooling dynamics and thermal interface resistance of glass-embedded metal nanoparticles, Phys. Rev. B 80 (19) (2009) 195406.

[25] T. Stoll, P. Maioli, A. Crut, S. Rodal-Cedeira, I. Pastoriza-Santos, F. Vallée, N. Del Fatti, Time-resolved investigations of the cooling dynamics of metal nanoparticles: impact of environment, J. Phys. Chem. C 119 (22) (2015) 12757–12764.

[26] M. Gandolfi, A. Crut, F. Medeghini, T. Stoll, P. Maioli, F. Vallée, F. Banfi, N. Del Fatti, Ultrafast thermo-optical dynamics of plasmonic nanoparticles, J. Phys. Chem. C 122 (15) (2018) 8655–8666.

[27] R. Rouxel, M. Diego, F. Medeghini, P. Maioli, F. Rossella, F. Vallée, F. Banfi, A. Crut, N. Del Fatti, Ultrafast thermo-optical dynamics of a single metal nano-object, J. Phys. Chem. C 124 (28) (2020) 15625–15633.

[28] C. Panais, R. Rouxel, N. Lascoux, S. Marguet, P. Maioli, F. Banfi, F. Vallée, N. Del Fatti, A. Crut, Cooling dynamics of individual gold nanodisks deposited on thick substrates and nanometric membranes, J. Phys. Chem. Lett. 14 (2023) 5343–5352.

[29] M.J. O'Connell, S.M. Bachilo, C.B. Huffman, V.C. Moore, M.S. Strano, E.H. Haroz, K.L. Rialon, P.J. Boul, W.H. Noon, C. Kittrell, J. Ma, R.H. Hauge, R.B. Weisman, R.E. Smalley, Band gap fluorescence from individual single-walled carbon nanotubes, Science 297 (5581) (2002) 593–596.

[30] D.H. Marsh, G.A. Rance, M.H. Zaka, R.J. Whitby, A.N. Khlobystov, Comparison of the stability of multiwalled carbon nanotube dispersions in water, Phys. Chem. Chem. Phys. 9 (40) (2007) 5490.

[31] S. Salassi, A. Cardellini, P. Asinari, R. Ferrando, G. Rossi, Water dynamics affects thermal transport at the surface of hydrophobic and hydrophilic irradiated nanoparticles, Nanoscale Adv. 2 (8) (2020) 3181–3190.

[32] H. Dang, D. Song, Z. Lin, M. An, W. Ma, X. Zhang, Effect of axial electric field on confined water in carbon nanotube: Enhancement of thermophoresis, Int. J. Heat Mass Transfer 190 (2022) 122751.

[33] F. Jabbari, A. Rajabpour, S. Saedodin, S. Wongwises, Effect of water/carbon interaction strength on interfacial thermal resistance and the surrounding molecular nanolayer of CNT and graphene flake, J. Mol. Liq. 282 (2019) 197–204.

[34] S. Alosious, S.K. Kannam, S.P. Sathian, B. Todd, Nanoconfinement effects on the kapitza resistance at water–CNT interfaces, Langmuir 37 (7) (2021) 2355–2361.

[35] A. Alexiadis, S. Kassinos, The density of water in carbon nanotubes, Chem. Eng. Sci. 63 (8) (2008) 2047–2056.

[36] M.H. Köhler, J.R. Bordin, C.F. de Matos, M.C. Barbosa, Water in nanotubes: The surface effect, Chem. Eng. Sci. 203 (2019) 54–67.

[37] X. Wei, T. Zhang, T. Luo, Thermal energy transport across hard–soft interfaces, ACS Energy Lett. 2 (10) (2017) 2283–2292.

[38] A. Casto, F.M. Bellussi, M. Diego, N. Del Fatti, F. Banfi, P. Maioli, M. Fasano, Water filling in carbon nanotubes with different wettability and implications on nanotube/water heat transfer via atomistic simulations, Int. J. Heat Mass Transfer 205 (2023) 123868.

[39] Y. Wang, H. Zhan, Y. Xiang, C. Yang, C.M. Wang, Y. Zhang, Effect of covalent functionalization on thermal transport across graphene–polymer interfaces, J. Phys. Chem. C 119 (22) (2015) 12731–12738.

[40] S. Chen, M. Yang, B. Liu, M. Xu, T. Zhang, B. Zhuang, D. Ding, X. Huai, H. Zhang, Enhanced thermal conductance at the graphene–water interface based on functionalized alkane chains, RSC Adv. 9 (8) (2019) 4563–4570.

[41] S. Lin, M.J. Buehler, The effect of non-covalent functionalization on the thermal conductance of graphene/organic interfaces, Nanotechnology 24 (16) (2013) 165702.

[42] S. Chatterjee, Paras, H. Hu, M. Chakraborty, A review of nano and microscale heat transfer: An experimental and molecular dynamics perspective, Processes 11 (9) (2023) 2769.

[43] C. Voisin, N. Del Fatti, D. Christofilos, F. Vallée, Ultrafast electron dynamics and optical nonlinearities in metal nanoparticles, J. Phys. Chem. B 105 (12) (2001) 2264–2280.

[44] N. Del Fatti, R. Bouffanais, F. Vallée, C. Flytzanis, Nonequilibrium electron interactions in metal films, Phys. Rev. Lett. 81 (4) (1998) 922–925.

[45] G.V. Hartland, Optical studies of dynamics in noble metal nanostructures, Chem. Rev. 111 (6) (2011) 3858–3887.

[46] R. Rouxel, M. Diego, P. Maioli, N. Lascoux, F. Vialla, F. Rossella, F. Banfi, F. Vallée, N. Del Fatti, A. Crut, Electron and lattice heating contributions to the transient optical response of a single plasmonic nano-object, J. Phys. Chem. C 125 (42) (2021) 23275–23286.

[47] G. Galimberti, S. Ponzoni, A. Cartella, M.T. Cole, S. Hofmann, C. Cepek, G. Ferrini, S. Pagliara, Probing the electronic structure of multi-walled carbon nanotubes by transient optical transmittivity, Carbon 57 (030) (2013) 50–58.

[48] B. Langlois, R. Parret, F. Vialla, Y. Chassagneux, P. Roussignol, C. Diederichs, G. Cassabois, J.-S. Lauret, C. Voisin, Intraband and intersubband many-body effects in the nonlinear optical response of single-wall carbon nanotubes, Phys. Rev. B 92 (15) (2015) 155423.

[49] F. Banfi, V. Juvé, D. Nardi, S. Dal Conte, C. Giannetti, G. Ferrini, N. Del Fatti, F. Vallée, Temperature dependence of the thermal boundary resistivity of glass-embedded metal nanoparticles, Appl. Phys. Lett. 100 (1) (2012) 011902.

[50] D.W. Hahn, M.N. Özişik, Heat Conduction, Wiley, 2012.

[51] C. Caddeo, C. Melis, A. Ronchi, C. Giannetti, G. Ferrini, R. Rurali, L. Colombo, F. Banfi, Thermal boundary resistance from transient nanocalorimetry: A multiscale modeling approach, Phys. Rev. B 95 (2017) 085306.

[52] C.F. Bohren, D.R. Huffman, Absorption and Scattering of Light by Small Particles, Wiley, New York, 1983.

[53] B. Stagg, T. Charalampopoulos, Refractive indices of pyrolytic graphite, amorphous carbon, and flame soot in the temperature range 25° to 600° C, Combust. Flame 94 (4) (1993) 381–396.

[54] H. Carslaw, J.C. Jaeger, Conduction of Heat in Solids, Clarendon, Oxford, 1959.

[55] D.P. Gulo, N.T. Hung, T.-J. Yang, G.-J. Shu, R. Saito, H.-L. Liu, Exploring unusual temperature-dependent optical properties of graphite single crystal by spectroscopic ellipsometry, Carbon 197 (2022) 485–493.

[56] M. Bruna, S. Borini, Optical constants of graphene layers in the visible range, Appl. Phys. Lett. 94 (3) (2009) 031901.

[57] A.B. Kuzmenko, E. van Heumen, F. Carbone, D. van der Marel, Universal optical conductance of graphite, Phys. Rev. Lett. 100 (11) (2008) 117401.
[58] A.S. Tascini, J. Armstrong, E. Chiavazzo, M. Fasano, P. Asinari, F. Bresme, Thermal transport across nanoparticle-fluid interfaces: The interplay of interfacial curvature and nanoparticle-fluid interactions, Phys. Chem. Chem. Phys. 19 (4) (2017) 3244–3253.
[59] O. Gutiérrez-Varela, S. Merabia, R. Santamaria, Size-dependent effects of the thermal transport at gold nanoparticle–water interfaces, J. Phys. Chem. 157 (8) (2022) 084702.
[60] D. Alexeev, J. Chen, J.H. Walther, K.P. Giapis, P. Angelikopoulos, P. Koumoutsakos, Kapitza resistance between few-layer graphene and water: liquid layering effects, Nano Lett. 15 (9) (2015) 5744–5749.
[61] Y. Ma, Z. Zhang, J. Chen, K. Sääskilahti, S. Volz, J. Chen, Ordered water layers by interfacial charge decoration leading to an ultra-low kapitza resistance between graphene and water, Carbon 135 (2018) 263–269.
[62] D. Konatham, A. Striolo, Thermal boundary resistance at the graphene-oil interface, Appl. Phys. Lett. 95 (16) (2009) 163105.